DISPERSION MEASUREMENT FOR ON-CHIP MICRORESONATOR

A Thesis

Submitted to the Faculty

of

Purdue University

by

Steven Chen

In Partial Fulfillment of the

Requirements for the Degree

of

Master of Science in Electrical and Computer Engineering

May 2015

Purdue University

West Lafayette, Indiana

TABLE OF CONTENTS

LIST OF TABLES

LIST OF FIGURES

ABSTRACT

Chen, Steven. M.S.E.C.E., Purdue University, May 2015.
Dispersion Measurement for On-chip Microresonator
Major Professor: Andrew M. Weiner

The cavity dispersion is an important factor to the generation of microresonator frequency comb. In order to find the dispersion for micro ring, we measure the dispersion by beating a tunable laser with a mode locked laser frequency comb. The measurement takes less than 10 seconds to complete and has decent accuracy. We developed the codes to process the raw data and calculate the cavity dispersion from the free spectral range evolution. From the experimental result, we were able to get to 10% uncertainty for the measurement on some micro-ring. In addition, we found that our measured dispersion match with the simulated value for a number of devices.

1. INTRODUCTION

1.1   Optical Frequency Comb

Optical frequency comb is consisted of a series of discrete and equal spacing component in frequency spectrum. The precise frequency component of frequency comb provides advantages in optical metrology [1] [2], high precision spectroscopy [3], advancement in GPS technology [4], and short pulse generation [5]. The frequency comb can be generated by the stabilization of mode locked laser and the frequency spacing between the comb corresponds to the repetition rate of the mode locked laser. Due to the difference between phase velocity and group velocity in laser cavity, an offset frequency called carrier offset frequency will be introduced. The frequency of individual component can be described by the following equation [6]:

$$f_m = m f_{rep} + f_{CEO} \qquad\qquad (1.1)$$

Where f_{rep} is the repetition rate of the frequency comb and f_{CEO} is the carrier offset frequency. Figure 1.1 shows the diagram of the frequency comb. The carrier offset frequency would introduce a delay in time domain, the delay will cause the peak of the carrier slips from the peak of the pulse envelope. This is illustrated in figure 1.1(b).
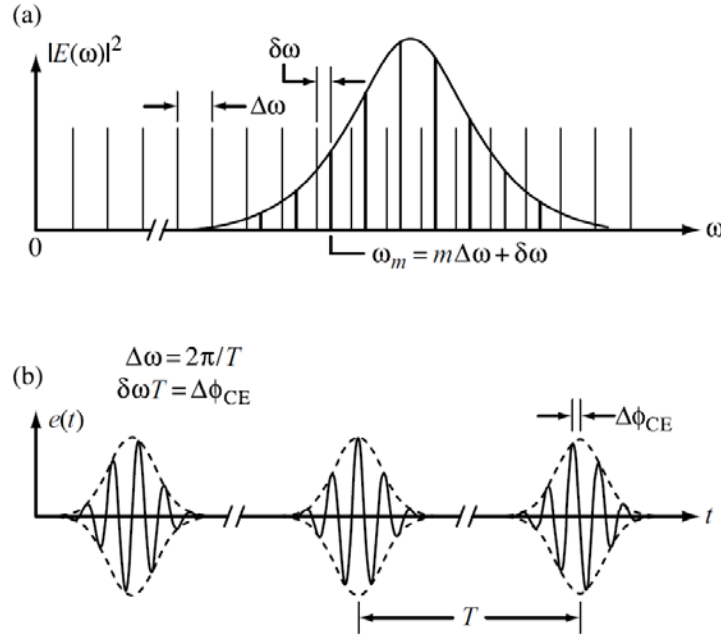
Figure 1.1 (a) Illustration of a frequency comb in frequency domain. (b) Time domain pulse of a frequency comb. Figure adopted from [6]

1.2   Dispersion

Dispersion is a phenomenon that different frequency components travel at different speed in a medium. For a short pulse travels in a dispersive fiber, the dispersion would broaden the pulse in time domain and thus distort the information. When light pass through a dispersive medium of length L, a phase will be introduced with the following relation [6]:

$$\varphi = -\beta(\omega)L \tag{1.2}$$

Where $\beta(\omega)$ is the propagation constant of the light. $\beta(\omega)$ can be express in Taylor Expansion as [6]

$$\beta(\omega) = \beta(\omega_0) + \frac{\partial \beta}{\partial \omega}(\omega - \omega_0) + \frac{1}{2}\frac{\partial^2 \beta}{\partial \omega^2}(\omega - \omega_0)^2 + \cdots \tag{1.3}$$

$\beta_1 = \frac{\partial \beta}{\partial \omega}$ is the inverse of group velocity and $\beta_2 = \frac{\partial^2 \beta}{\partial \omega^2}$ is the dispersion term. We can see this by considering β_2 introduce a quadratic phase, which corresponds to a frequency dependent time delay. The delay can be expressed as [6]

$$\Delta\tau(\lambda) = \frac{-2\pi c \beta_2 \Delta\lambda L}{\lambda^2} \tag{1.4}$$

The delay is related to the dispersion term D by $\Delta\tau(\lambda) = D\Delta\lambda L$, so we can expressed D by

$$D = \frac{-2\pi c \beta_2}{\lambda^2} \tag{1.5}$$

1.3   Microresonator Frequency Comb and the Relation to Dispersion

Recently, a new way to generate frequency comb from pumping continuous wave (CW) laser to the high quality factor (Q) micro resonator has been demonstrated [7] [8] [9]. This type of frequency comb has the advantage of compact, low power, and CMOS compatible. In addition, the repetition rate of micro-resonator frequency comb can easily reach tens GHz range, which is higher than conventional frequency combs [8]. When the laser wavelength is tuned into one of the resonance of the micro-ring, the intracavity power in the high-Q resonator will build up and create nonlinear four wave mixing (FWM) effect. FWM is a third order nonlinear effect, which involves refractive index being dependent to the power of the light beam. The FWM can be described as the energy of two pump photons is converted to signal photon and idler photon that follows the equation [8]:

$$2\omega_p = \omega_s + \omega_i \tag{1.3}$$

With $\omega_s = \omega_p + \Omega$ and $\omega_i = \omega_p - \Omega$. ω_s and ω_i are the generated sideband. The sideband would again generate FWM, and additional sideband will be generated. The process is called cascaded FWM. The frequency components of the comb correspond to the FSR of the micro-resonator.

Cavity dispersion is strongly related to the micro-resonator frequency comb. It is related to the formation of micro-resonator frequency comb [10] [11]. By tuning the cavity dispersion, initial sideband can be adjusted between single free spectral range (FSR) or several FSR away. The single FSR combs are termed type I comb, whereas the frequency comb which initial sideband are several FSR away are called type II comb [12] [13] . By further detuning the laser into resonance, additional sideband will appear for type II combs. Type I combs are coherent and noise free, which is ideal for optical communications [12]. Type II combs are initially coherent when the comb spacing are several FSR away; however, when the laser wavelength is further tuned into the resonance, additional sideband will be generated but the comb become incoherent [12]. Cavity dispersion will affect the bandwidth of the frequency comb as well. It has been shown that micro-resonator frequency combs can reach octave if the dispersion is optimize [14] d [15].

Finally, the formation of temporal soliton is related to cavity dispersion as well. Bright soliton can be generated with the aid of modulation instability (MI) in anomalous dispersion regime [16] [17] as well as normal dispersion regime [18]. In contrast, dark soliton is generated in normal dispersion regime with the aid of mode interaction.

2. DISPERSION MEASUREMENT EXPERIMENT

In this chapter we will introduce the basic measurement technique and the apparatus that will be used in the experiment. In Section 2.1.1 we will introduce the formalism for retrieving microresonator cavity dispersion from the free spectral range (FSR) of the transmission spectrum. In Section 2.1.2 we will briefly discuss about the idea of precise measurement of cavity dispersion. In Section 2.2, the experimental setup to measure dispersion is introduced. Then we will discuss about the choice of setting and characteristic of the instruments in Section 2.3. Finally, the algorithm of processing raw data captured by the oscilloscope will be introduced in Section 2.4 and 2.5.

2.1   Microresonator Dispersion Measurement Theory

2.1.1   Derivation of Cavity Dispersion from FSR evolution

We will briefly introduce the idea for measuring cavity dispersion here. In order to measure the dispersion, it is required to obtain the transmission spectrum of the microresonator. The transmission spectrum is obtained by sweeping a tunable laser within certain wavelength range through the micro-resonator. We then find the FSR between resonance peaks and calculate the dispersion. Figure 2.1 shows a typical transmission spectrum. Here we sweep the tunable laser from 1530nm to 1570nm. There are two modes in this micro-ring. If the dispersion of the two modes is the same, the two modes will maintain same spacing over the spectrum. However, since the dispersion of the two modes is different, the two modes will cross each other along the spectrum.
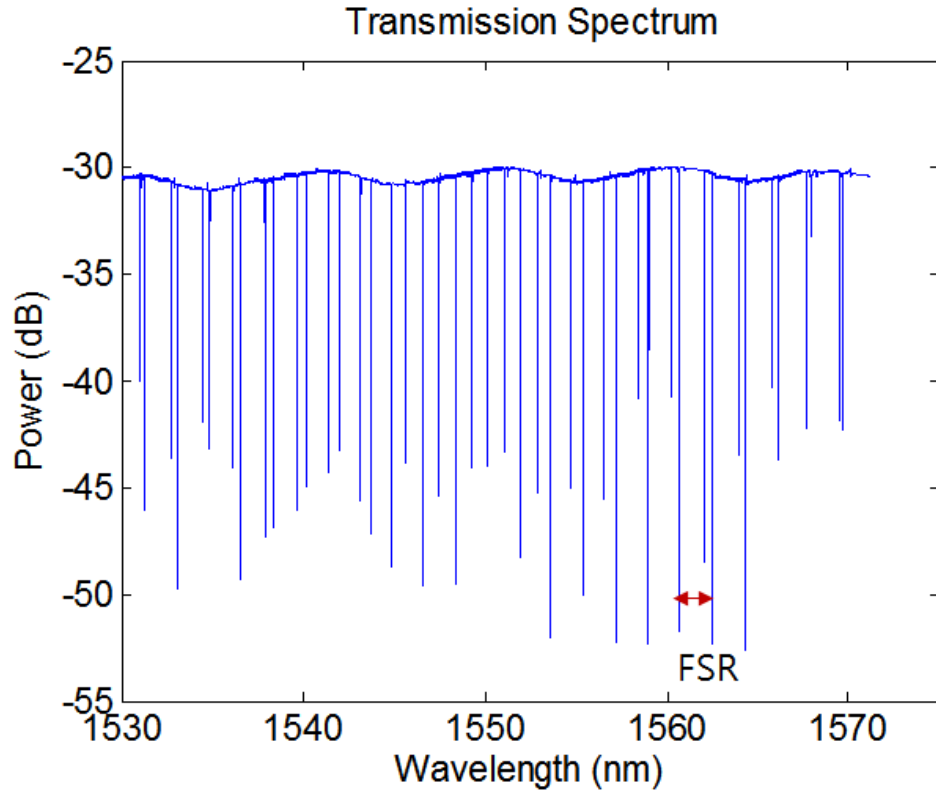
Figure 2.1 Transmission spectrum obtained by sweeping a tunable laser through a micro-ring. The FSR of the resonance is also indicated.

Now we would like to find the relation between FSR and cavity. The phase between any two frequencies can be expressed as

$$\varphi - \varphi_0 = -\beta(\omega)L - (-\beta(\omega_0)L) \tag{2.1}$$

Use the equation in (1.2), we can find that

$$\varphi - \varphi_0 = -L(\beta_1 * (\omega - \omega_0) + \frac{\beta_2}{2} * (\omega - \omega_0)^2) \tag{2.2}$$

where β_1 is related to the group velocity and β_2 is the dispersion term. Differentiating φ with respect to ω would yield

$$\frac{\Delta\varphi}{\Delta\omega} = -L(\beta_1 + \beta_2(\omega - \omega_0)) \tag{2.3}$$

Now we would like to relate $\Delta\varphi/\Delta\omega$ to FSR of the transmission spectrum. The phase difference between any two adjacent resonances is 2π; therefore, the ratio of $\Delta\varphi/\Delta\omega$ can be expressed as

$$\frac{\Delta\varphi}{\Delta\omega} = \frac{2\pi}{2\pi * FSR} = \frac{1}{FSR} \tag{2.4}$$

Finally, equating formula in 2.3 and 2.4, and taking the first two terms in Taylor series expansion we would get

$$FSR = \frac{1}{L} * \frac{1}{\beta_1 + \beta_2(\omega - \omega_0)} = \frac{1}{\beta_1 L} - \frac{\beta_2(\omega - \omega_0)}{\beta_1^2 L} \tag{2.5}$$

We then obtain the fitting coefficient for FSR. Suppose $FSR = a_1(\omega - \omega_0) + a_0$, then coefficient will be

$$a_{1=} - \frac{\beta_2}{\beta_1^2 L}, a_{0=}\frac{1}{\beta_1 L} \tag{2.6}$$

Rearranging the terms to express β_2 in a_0 and a_1:

$$\beta_2 = \frac{-a_0^2 * a_1}{L} \tag{2.7}$$

We can use equation (1.5) to obtain dispersion value D.

Previously, we used Agilent 8164 light wave measurement system to obtain the transmission spectrum and calculate the dispersion. However, the transmission spectrum sweeps takes about 30 minutes to complete from 1530nm to 1570nm. While the resonances will drift with the temperature change or even the vibration of the stage

during the measurement time, a precise measurement is not possible. Therefore, we could not obtain a reasonable dispersion value.

2.1.2 Precise Measurement of Cavity Dispersion

Recently, a method to measure cavity dispersion precisely has been demonstrated with the aid of frequency comb [3]. The measurement takes about four seconds to complete, which makes the FSR shift due to temperature negligible. The idea is to beat an optical frequency comb with a tunable laser. Figure 2.1 shows the setup for the measurement. A tunable laser is set to sweep mode to sweep over certain wavelength range. The optical frequency comb has precise frequency components every 250MHz.
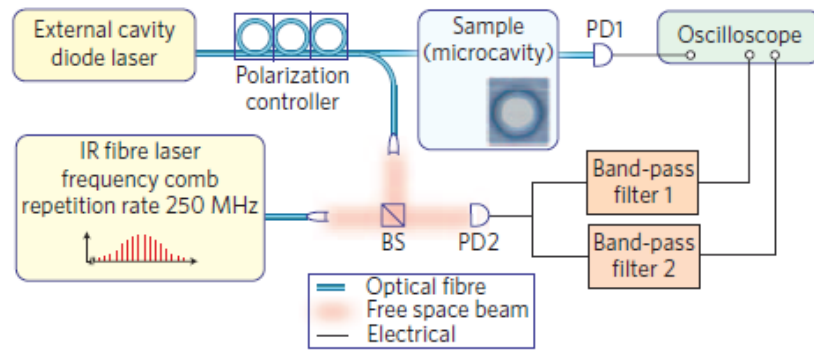
Figure 2.2 Experimental setup for measuring dispersion, reproduced from [3]

As the tunable laser frequency sweeps and approaches one of the comb line of frequency comb, a radio frequency beat signal will be generated. The radio frequency signal is converted to electrical signal by a photodiode, and the signal is fed into two narrow band band-pass filters. Therefore, for every frequency comb repetition rate f_{rep}, there will be four frequency markers generated at $f_{rep}+f_{BP1}$, $f_{rep}-f_{BP1}$, $f_{rep}+f_{BP2}$, and $f_{rep}-f_{BP2}$. As the tunable laser sweeps, frequency markers will be generated with the transmission spectrum of the microresonator. Thus the relative frequency spacing between the cavity resonances in the transmission spectrum can be obtained from these frequency markers. Figure 2.2 is a simple illustration that shows the frequency marker generated when the tunable laser beat with a comb line of frequency comb.
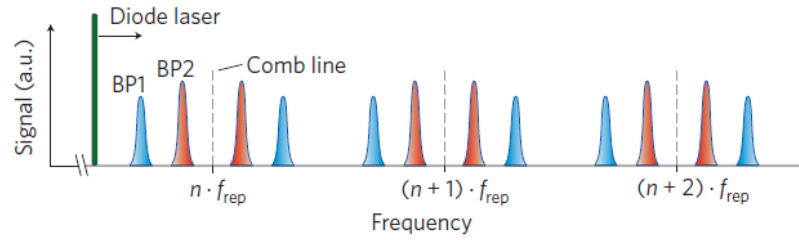
Figure 2.3 Illustration of the frequency marker created when the diode laser beat with frequency comb, reproduced from [3]

2.2 Experiment Setup

We use a similar experiment setup as described above. In our experimental, we used New Focus tunable laser as the primary laser source. The laser has maximum sweeping range from 1520nm to 1570nm and has advantage of small linewidth ($\leq$200kHz). The frequency comb is provided by MenloSystems optical frequency comb. The comb has repetition rate of 250MHz. Finally, we use Koheras fixed wavelength laser as reference to retrieve absolute frequency of the markers. Figure 2.4 shows the schematic diagram of the setup. We coupled fixed wavelength laser with the optical frequency comb. A polarization controller (PC) is used to adjust relative polarization of fixed wavelength laser relative to the optical frequency comb. Changing the polarization will also change the power coupled to the frequency comb. Tunable laser is set to the sweep mode and the sweeping range is set to 1520nm to 1570nm. A 50:50 coupler is placed after the tunable laser. 50% of the light will beat with the optical frequency comb to create frequency markers, the other 50% is sent into the micro ring so that the transmission spectrum is generated synchronously with the frequency markers. A balanced detector is used to reduce the common noise in the beat signal. A low pass filter is used to filter out is placed after the balanced detector to filter out the unwanted higher frequency in the beat signal. Two narrow band band-pass filters are placed after the balanced detector and low pass filter to generate frequency markers. The band-pass filters center at 30MHz and 75MHz each. Therefore, for every m*250MHz, we would have 4 frequency markers at m*250MHz±75MHz and m*250MHz±30MHz.
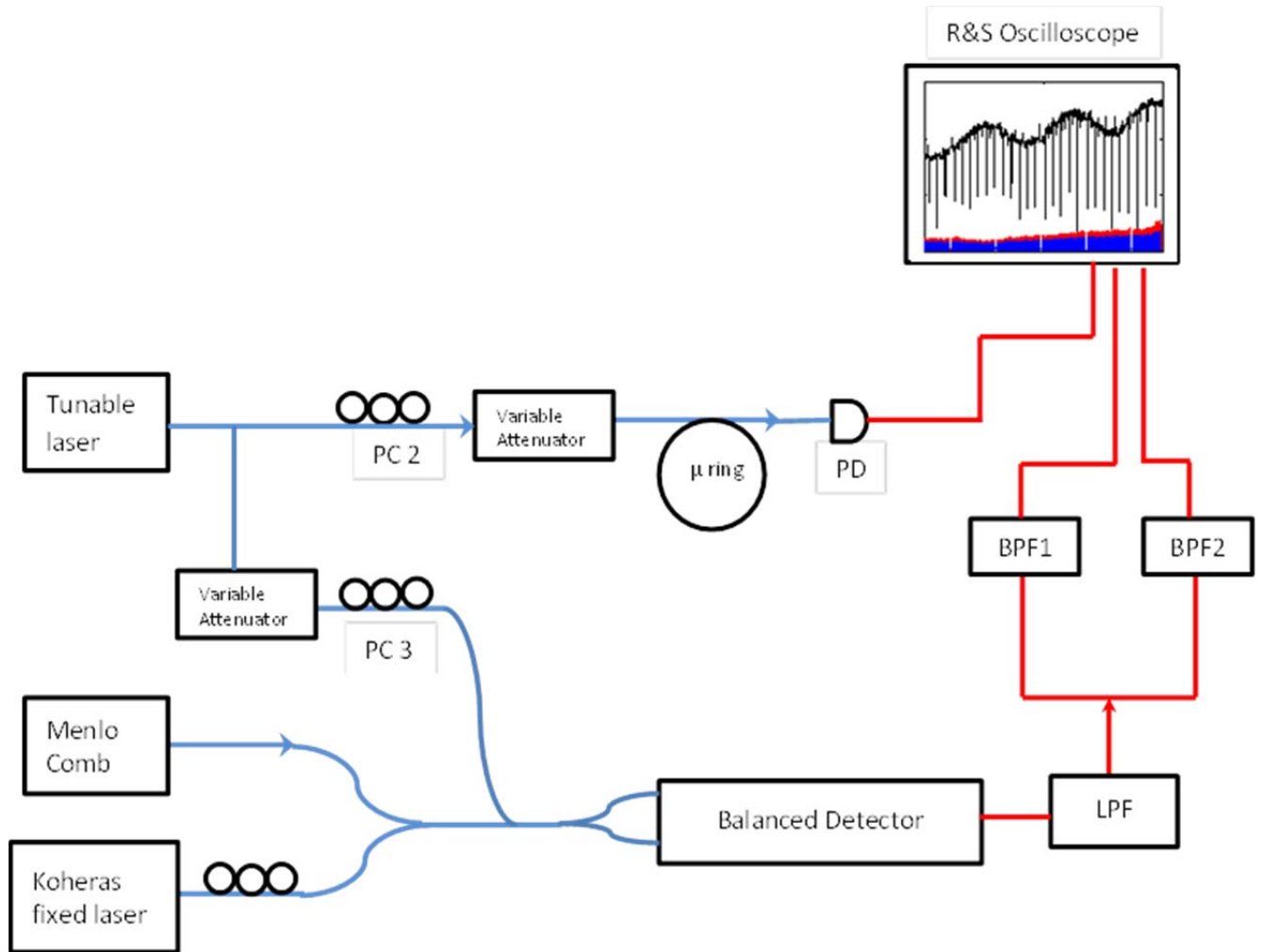
Figure 2.4 Experimental Setup for dispersion measurement. PC: Polarization Controller. PD: Photodiode. BPF: Band-pass Filter.

Since the tunable laser is sweeping continuously and we can't read wavelength at any instance, we are not able to retrieve the exact frequency of frequency markers. Therefore, we use a fixed wavelength laser as a reference to find the absolute frequency of the frequency markers. Four markers will be generated when the tunable laser wavelength is close to the wavelength of the fixed wavelength laser. In order to distinct these frequency markers from those generated from the beats between tunable laser and the optical frequency comb, we would adjust the polarization controller and variable attenuator until we see the reference markers that have greater amplitude compared to other frequency markers.

2.3   Equipment Characteristic and Setting

In this section, we will discuss about the setting for the tunable laser and the frequency response of the filters will be verified. We will also verify the output wavelength and the uncertainty of the reference laser. Finally, the setting of the oscilloscope will be reviewed.

If the experiment setup is correct, the resonances will be symmetric. The asymmetric resonances usually result from the input laser power is too high or the laser sweep speed is too fast. As described in [19], if the input laser power is too strong, the resonance will be red shifted. Figure 2.4 shows the comparison between symmetric resonance and asymmetric one. In figure 2.4(b), since the peak location of the asymmetric resonance will not be at the center of the resonance, extra error will be introduced to the FSR, and thus affects the dispersion. In order to keep the resonance symmetric, we would usually adjust the variable attenuator so that the power before entering micro ring to around -30dBm to -25dBm, which corresponds to 1μW to 3.16μW.
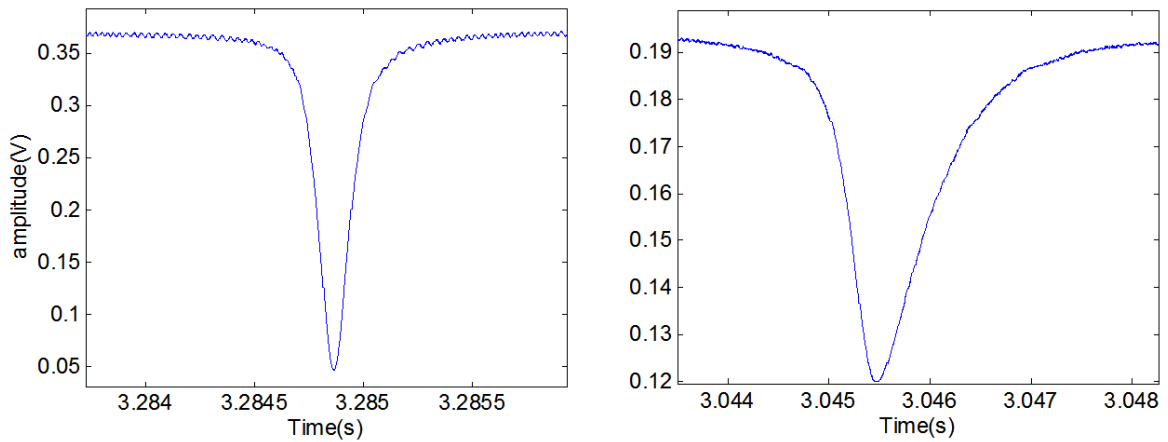
Figure 2.5 (a) A symmetric resonance captured by the oscilloscope. (b) Shows an asymmetric resonance.

In order to ensure the resonance are symmetric, we have to make sure the rise time of the photo-detector used to obtain the optical spectrum is shorter than the time it takes to sweep over any resonance. We set the laser sweep speed to 11nm/s and would like to know if the sweeping speed is too fast. First, we want to make sure that the Q factor is not degraded by the photodiode rise time. That is, we can't obtain the highest Q factor because the photodiode rise time is long compared to laser sweep speed. By fitting the resonance with Lorentzian curve, we are able to find the full width half maximum (FWHM) of the resonance, and the Q factor of the resonance is calculated by:

$$Q = \frac{f}{\Delta f_{FWHM}} \tag{2.8}$$

We found that the Q factor of the resonance shown in figure 2.6 is around 10^6, which match with the value obtained before. Now we would like to know how long it takes for the laser to sweep over this wavelength range. This can be easily checked on the oscilloscope and we found that the time is about 300μs as shown on figure 2.7. As defined in the datasheet of the photo-diode we used for capturing transmission spectrum, the rise time of the photo-detector can be calculated by:

$$t_R = 0.35 * (2\pi * R_{Load} * C_J) \tag{2.9}$$

C_J is the diode capacitance as defined in the specification sheet and we used a 100kΩ resistor for R_{Load}. The rise time of the photo-detector is found to be 4.84 μs. Therefore, the resonance is symmetric and we conclude that it is reasonable to set laser sweep speed to 11nm/s.
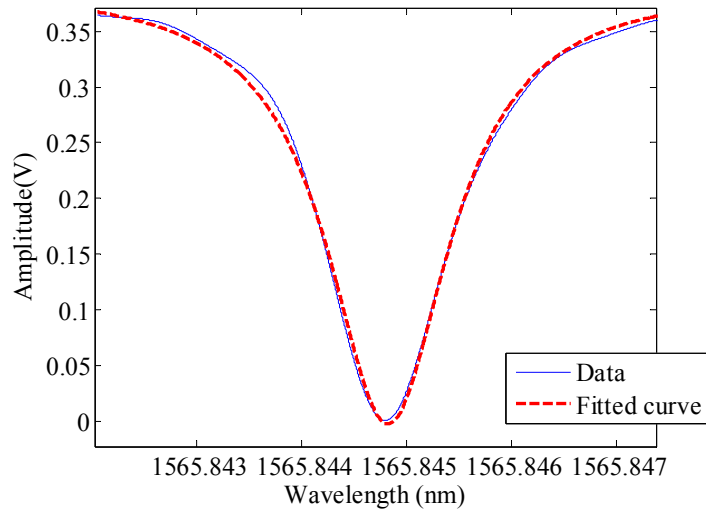
Figure 2.6 Curve fitting with Lorentzian distribution. The Q factor of the resonance is found to be around 10^6.
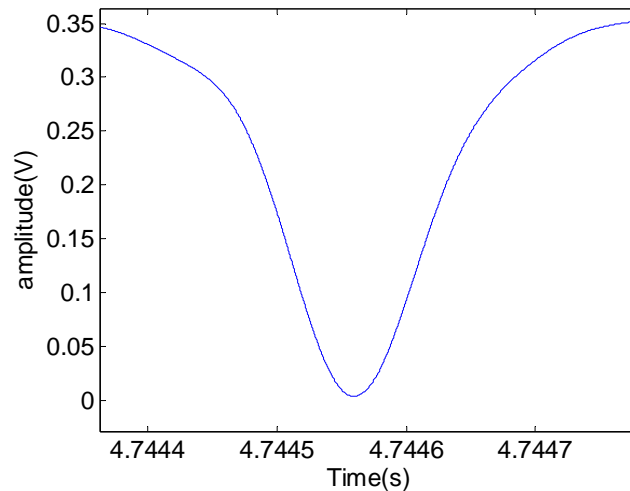
Figure 2.7 The resonance is captured in oscilloscope. It takes about 300μs to sweep over this resonance when the laser sweep speed is 11nm/s.

Next we would like to check the frequency response of the band-pass filter and low-pass filter. As mentioned above, we are using narrow-band band-pass filters to get frequency markers. The pass band is of interest to us. We use Agilent vector network analyzer (VNA) to test the frequency responses of both band-pass filters. Figure 2.7 is the response of the 75MHz and 30MHz band-pass filters. The -3 dB pass band is tested to be 1.19MHz for 75MHz band-pass filter and 1.39MHz for 30MHz band-pass filter.
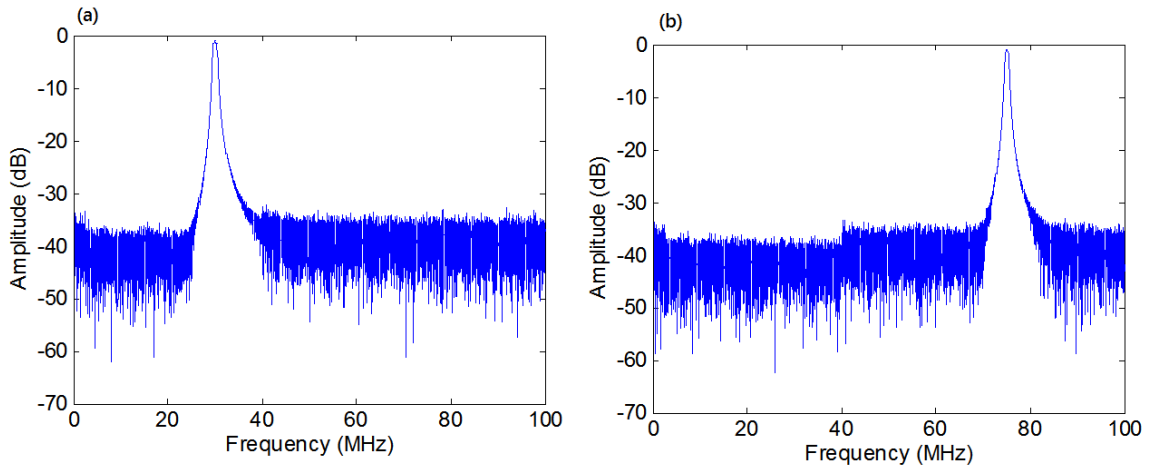
Figure 2.8 Frequency response of the band-pass filter used for frequency markers. (a) The response of 30MHz band-pass filter. (b) The response of 75MHz band-pass filter.

Next we would like to check the frequency response of the low-pass filter. The frequency response of the low pass filter is important since we want to make sure that higher beat frequency generated by mixing diode laser and Menlo comb won't overlap.. Figure 2.9 shows the frequency response of the low pass filter. The -3dB pass band of the low-pass filter is 118.15MHz.
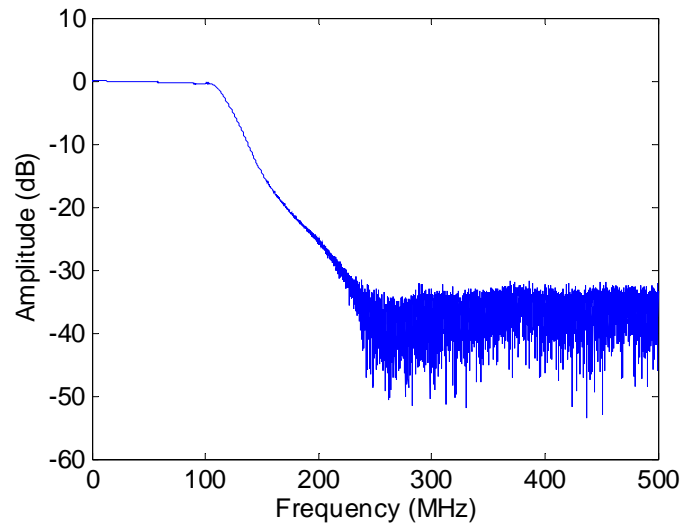
Figure 2.9 Frequency response of the low pass filter.

We used a fixed wavelength laser to retrieve the absolute frequency of the frequency markers and transmission spectrum of the micro-ring. Therefore, we would like to know the output wavelength and the stability of the laser. We used wavelength meter to measure the wavelength of the fixed laser around 5 minutes. The result is shown in figure 2.10. The average wavelength over the time interval is 1541.76206 nm and the uncertainty is 0.000038nm.
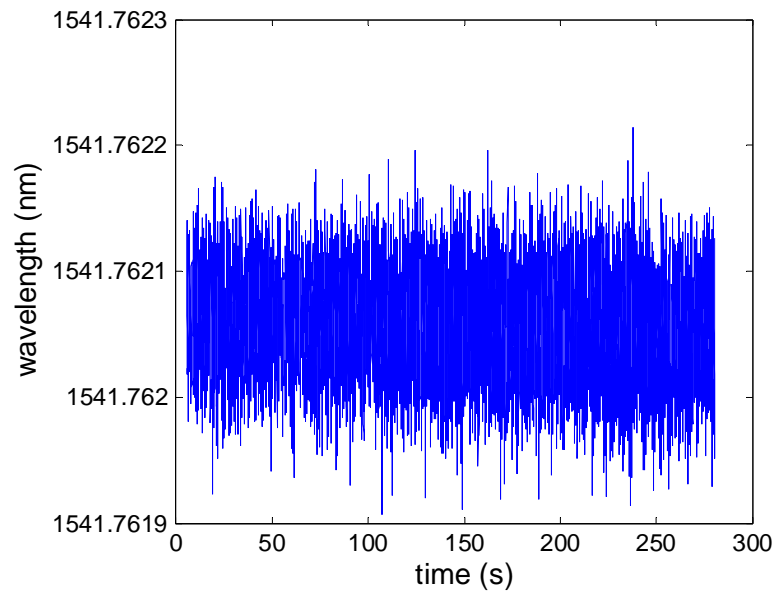
Figure 2.10 The wavelength variation of the fixed laser around 5 minutes. It is found that the wavelength is around 1541.76206±0.000038nm.

Finally, we would like to discuss about the setting for the oscilloscope. We used Rhode & Schwarz RTO oscilloscope for the experiment. We want to make sure that there is enough sample points for sampling both the transmission spectrum and the frequency markers. The sampling frequency is fast enough as long as there are more than two (which is the worst case scenario) sample points for each frequency marker. We determined the required sampling rate through experiment and found that it will be enough if the sampling rate is greater than 2.5M sample per second. It is observed that there are around 10 points for one frequency marker, and the maximum of the frequency marker can be captured. In order to get the frequency markers correctly, we have to set those 2 channels to peak detect mode. The peak detect mode will record the maximum and minimum value of the signal over the sampling time interval. The oscilloscope has two load impedance with 50Ω and 1MΩ each. In order to increase to signal to noise ratio (SNR) of both the transmission spectrum and frequency marker, we would prefer the 1MΩ resistor over the 50Ω resistor. For the transmission spectrum, we would put a parallel resistor of 100 kΩ to reduce the load resistor and shorten the rise time of the photo detector.

2.4   Algorithm for Processing Frequency Marker Data

In this section, we would like to introduce the algorithm for retrieving the frequency markers and resonance frequency from the transmission spectrum. Either missing a frequency marker or mistaking a noise as a frequency marker will make the resonance frequency erroneous.

First, in order to distinguish the marker from the noise background, we have to define a threshold that we would recognize a marker is present if the amplitude is greater than the threshold. However, the threshold can't be set too high that we might miss some frequency marker. Therefore, we use a moving average threshold that will be adjusted dynamically according to the local frequency marker amplitude. The dynamic average is useful because the power of the frequency comb and the tunable laser would increase from 1530nm to 1570nm. Therefore, the amplitude of the frequency markers has 3 times greater amplitude at 1570nm than 1530nm. The moving average threshold is used to reduce the chance of finding error marker.

We would like to discuss how we find the peak of the frequency marker here. The process is shown in Figure 2.11. We find the index where the amplitude is higher than the threshold and define it as the start of the frequency marker, which is point A in the figure. Then we define the index of the end of frequency marker B by finding the location where the amplitude is lower than the threshold after point A. This is the range of a frequency marker, and we simply find the local maximum between these 2 indexes to get the frequency marker peak. However, we would like to jump over certain range after we find a frequency marker peak to avoid recognizing the transient response of the band-pass filter as a marker. If the sampling rate is around 2.5M sample/s, the jump range of 10~15 samples will be enough. Finally, we use this index as the starting point to find next frequency marker peak, and the process repeat until we reach the end of data captured by the oscilloscope.

(a)   (b)
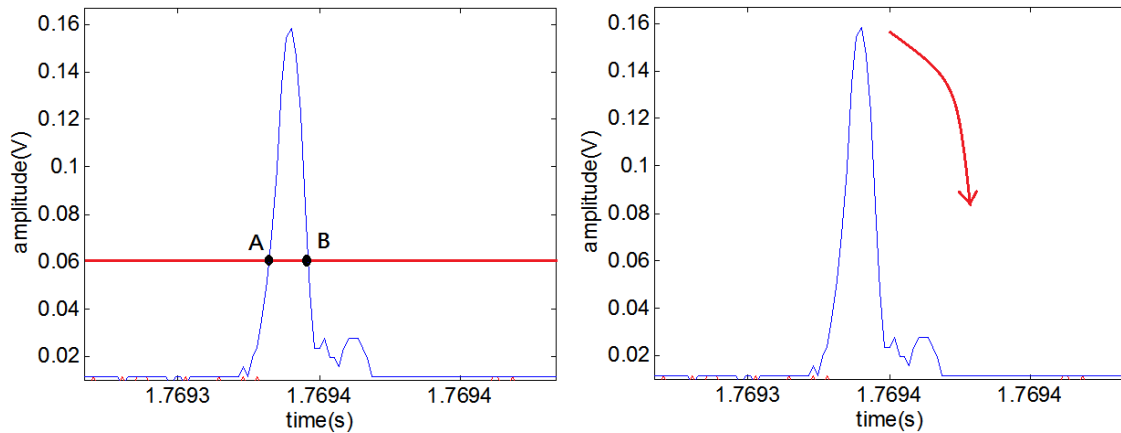
Figure 2.11 (a) A minimum threshold is set to distinguish frequency marker from noise background. Point A is defined to be start of a frequency marker and B is end of frequency marker. (b) A small jump is introduced to avoid the transient response of the band-pass filter is captured as well.

After the peak finding process is complete, we have to check if there are either missing markers or noise peak being recognized as a marker. We define -75MHz, -30MHz, 30MHz, and 75MHz frequency markers relative to a comb line of the frequency comb as a set. Figure 2.12 shows a set of frequency markers. We can determine if there is any acquisition error if we check the relative position between 30MHz peaks and 75MHz peaks. Referring to figure 2.12, if we get one full set, the index difference of (peak2-peak1), (peak3-peak1), (peak 4-peak 2), and (peak 4-peak 3) will be positive. We can perform this check for every set of 4 frequency markers we acquired and the error can be detected if any of the difference changes sign. If one of the peaks has smaller amplitude and not recognized as a marker as shown on figure 2.13, the index difference (peak 4-peak 3) will be negative, and we can tell one of the 30MHz peak is missing.

Figure 2.12 Example of one set of frequency marker. No error if peak (1) to (4) is in the right order.

Figure 2.13 First 30MHz peak has smaller amplitude and is not recognized as a marker. The index difference of (4)-(3) will be negative and we can tell one of the peak is missing.

Now, we would want to discuss how we are going to find frequency markers near reference frequency markers that generated by the fixed wavelength laser. In order to distinct the reference frequency marker from others, we set the power of the reference marker higher than any other frequency markers. Figure 2.14 illustrates the frequency markers near the reference. The location of the peak can be determined by using the same technique for finding other markers. Since the reference marker power is stronger than other markers, it will be included when we retrieve normal markers. There are two ways

to rule out these markers: first is compare the amplitude of reference markers to normal threshold. If it is several times higher, we can determine that this is a reference marker. The other way we can simply check the index of the smaller amplitude frequency markers we found and compare with the index of reference marker we already known.
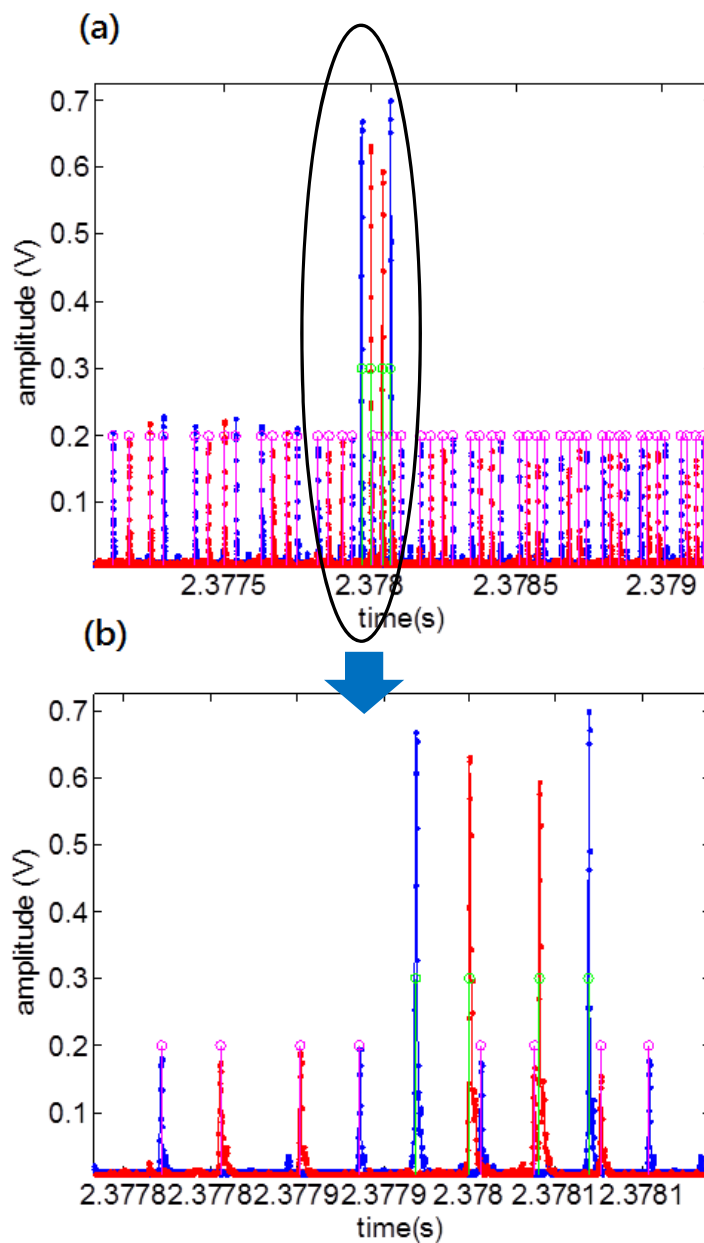
Figure 2.14 (a) Frequency markers near the reference marker. The magenta circle represents the frequency markers retrieved. The light green circle is the reference markers. (b) Zoom in picture of the frequency marker where the marker almost overlaps with the reference. Since they don't actually overlap, we can retrieve this marker without error.

One problem that would occur with this setup is when the reference peaks overlap with normal frequency markers. In that case, we will have a missing marker. To solve this problem, we can calculate the index spacing between the reference markers we already know. Although the laser sweeping speed is not constant during the scan, the reference markers and local frequency markers are close enough that we can consider they have same sweep speed. Therefore, we can use the index spacing between reference markers to predict the location of the missing one. If there is a reference marker near that location, we assume that those 2 markers overlap.

Occasionally, we observe noise beat note in our data. The beat note would have similar amplitude to the frequency marker and make it hard to distinguish noise beat note from the marker. With some trial and error, we determine that it is due to the locking state of Menlo comb. This problem can be solved by relocking Menlo comb.

2.5   Algorithm for Processing Transmission Data

The algorithm for finding cavity resonances is similar to that for the frequency marker. However, since there is more uncertainty in the transmission data, we have to manually determine several parameters. First, there is high-frequency noise present in the transmission data, so we utilize digital low-pass filter to smooth the spectrum. In addition, sometimes we would observe change in transmission background power that is caused by either tunable laser or variable attenuator. Therefore, we will filter out a small part of low frequency components near DC of the transmission data to make the background flatter. To find the location of the cavity resonance, we use similar technique to finding the frequency markers. A threshold will be defined, but the threshold is manually determined since every device has different coupling loss and we usually have different power at the photo-detector. Occasionally, we will observe some of the resonances have very small extinction. Therefore, we have to add some of the resonances manually when it occurs.

A major difficulty that limits our ability to find dispersion accurately is the double peaks at the resonance peak. We observe that there are double peaks at some resonance

peaks in a number of micro-resonators. The splitting of the resonance peak may result from backward propagating wave induced by the scattering of light at coupling region or surface roughness [20]. In such case, we will not be able to find the exact location of the resonance peak. Figure 2.10 shows a resonance with double peak. We used 2 methods to overcome this issue. One choice is the fit the resonance. By fitting the resonance with the Lorentzian function, we may be able to find the peak of the resonance even if there is a double peak present. The second choice is not to take the resonance into account. However, this method sometimes would make the curve fitting unreliable. Therefore, the first method is preferred over the second one.
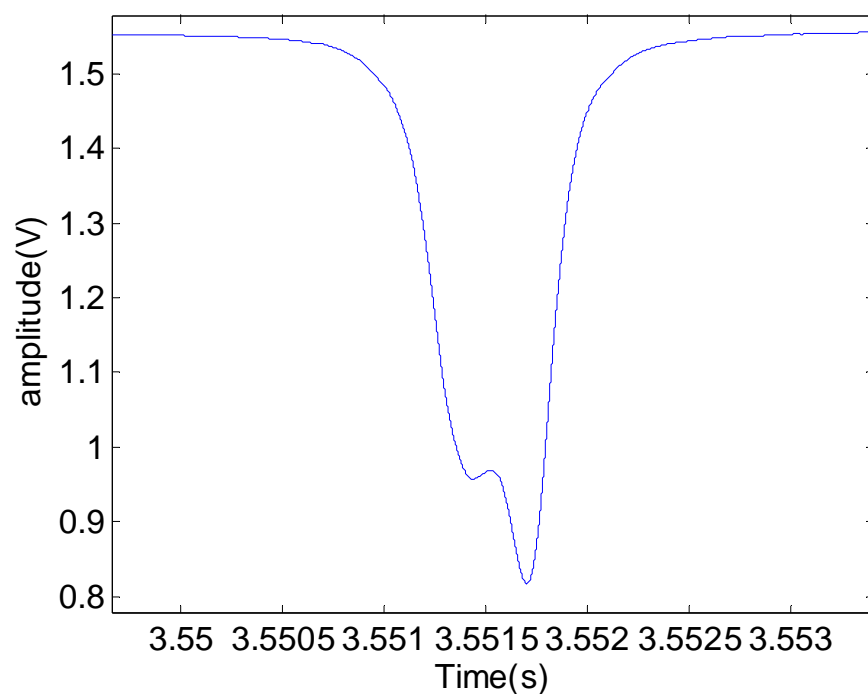
Figure 2.10 Double peak resonance is sometimes found in the transmission spectrum. The location of peak can't be determined.

3. EXPERIMENTAL RESULT

In this chapter we will discuss the dispersion measurement result we obtained. The majority of the device we measured has waveguide height of 550nm, 595nm, and around 800nm. In general, we would expect the dispersion to be normal dispersion for 550nm device and anomalous dispersion for 800nm device. The device with 595nm waveguide-height devices has dispersion falls in between. In addition, the uncertainty of the dispersion measurement will be discussed. We were able to have accurate measurement for some of the devices. Finally, we will briefly discuss the mode coupling phenomena. It was observed that when two different modes cross each other, the local dispersion would be modified.

3.1   Dispersion of Different Waveguide Dimension

We would like to show some dispersion measurement results in this section. The first micro-ring sample has waveguide height of 430nm, and waveguide width of 2 μm. The ring radius is 200 μm. Figure 3.1 shows the microscopic figure of the microring and cross-section of the waveguide. The silicon nitride is deposited on top of silicon dioxide substrate, and then the top of waveguide is covered with a silicon dioxide layer. Figure 3.2(a) shows the transmission spectrum of the device. One of the resonances was found to be double peak. The zoom-in picture of the double peak is shown in figure 3.2(b). The transmission spectrum in figure 3.2 is reconstructed with the retrieved frequency markers. Since we didn't use reference laser while doing this measurement, the frequency is relative frequency instead of exact frequency.

(a)

(b)
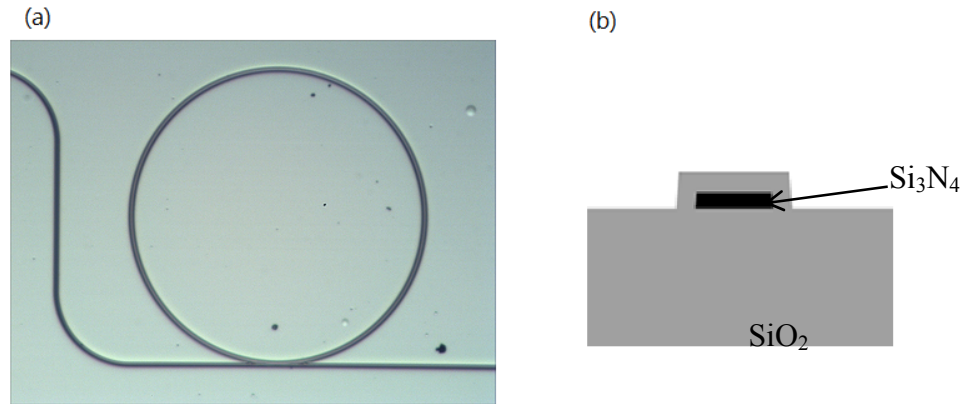
Figure 3.1 (a) Microscope view of the micro-ring. (b) Cross-section illustration of the micro-ring.
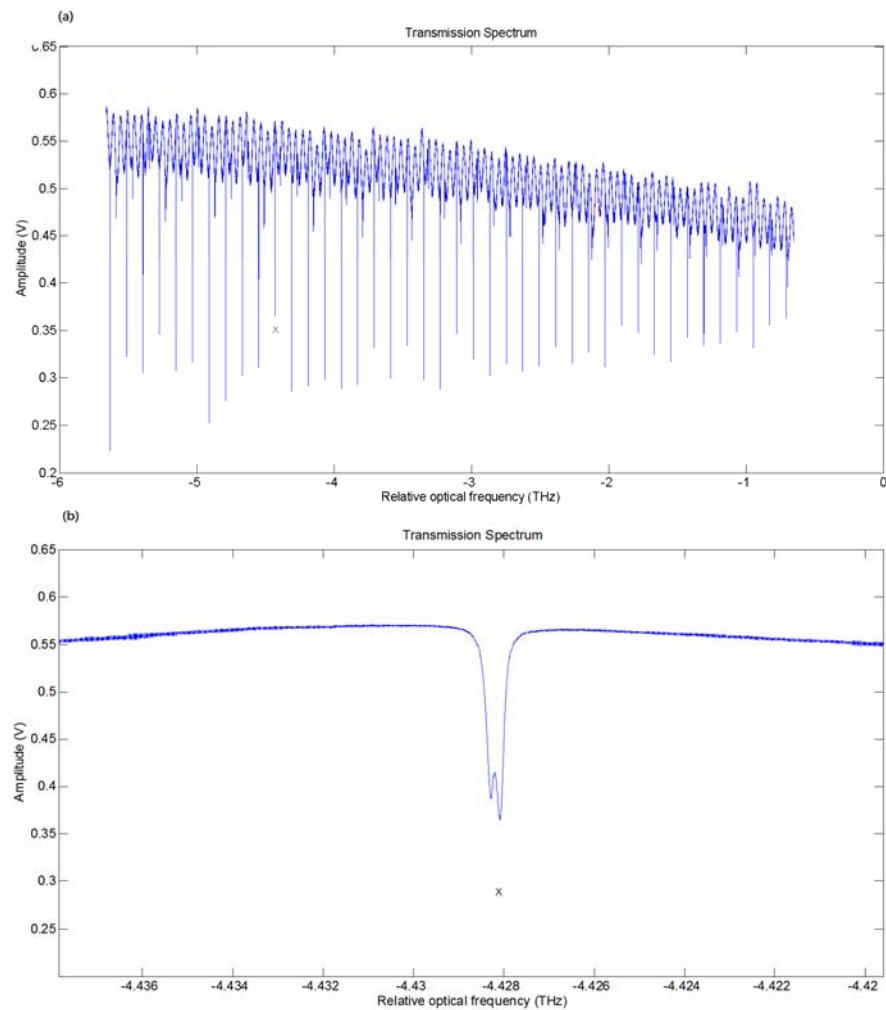
Figure 3.2 Transmission spectrum of the device with 430nm × 2μm dimension. (a) The transmission spectrum of the device. The x axis is the relative frequency obtained by frequency marker. The real frequency is unknown since the reference laser wasn't included. (b) Zoom in view of the peak mark as 'x' in (a). The peak has double peak feature, so we exclude that from our FSR fitting.

It is obvious that only 1 mode with significant extinction ratio, so the FSR retrieval is trivial. FSR evolution is shown in Figure 3.3. By fitting the curve of FSR evolution, we obtained the dispersion of this device to be -1058.7 ps/nm/km. The negative value means that the micro-resonator has normal dispersion. We can figure out if the micro-ring has either normal or anomalous dispersion from the FSR evolution. If the FSR is decreasing with higher frequency, we can interpret that as the refraction index is increasing as the frequency increase, which is the definition of normal dispersion. In contrast, if the FSR is proportional to the frequency, the micro-ring has anomalous dispersion.
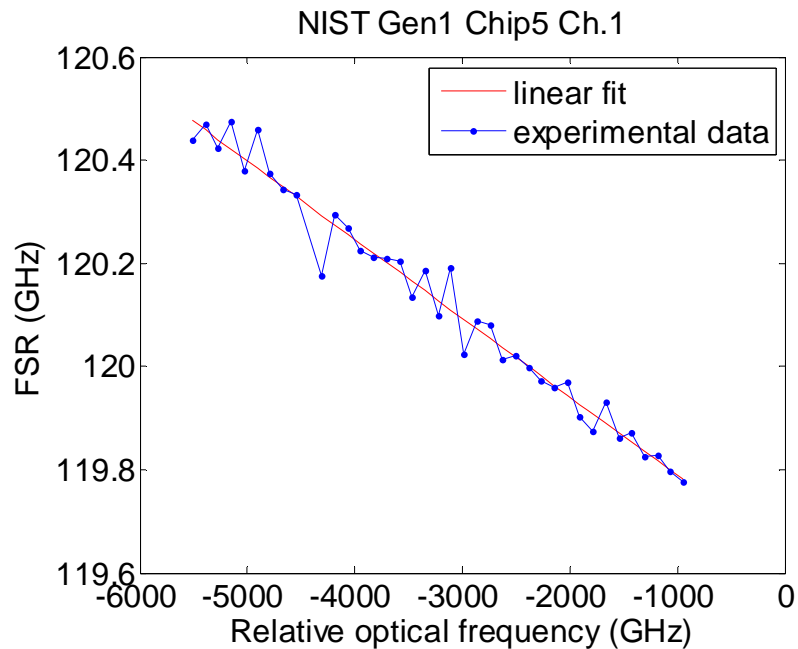
Figure 3.3 FSR evolution and the fitting curve of the experimental data. Dispersion can be calculated from the parameters of the curve fitted.

Next we would like to show the measurement result of a device with multiple modes. When there is more than one mode, we have to group resonances to the same mode family. The micro-ring we tested has waveguide height of 790nm, waveguide width of 2μm, and the ring radius is 100μm. The raw data we acquired is shown in figure 3.4. The x-axis of the figure is time on the oscilloscope. The time it takes to capture all data is around 4.55 second since we set the sweep speed to 11nm per second, and we set time range to 4.7 second to ensure every resonances is included.
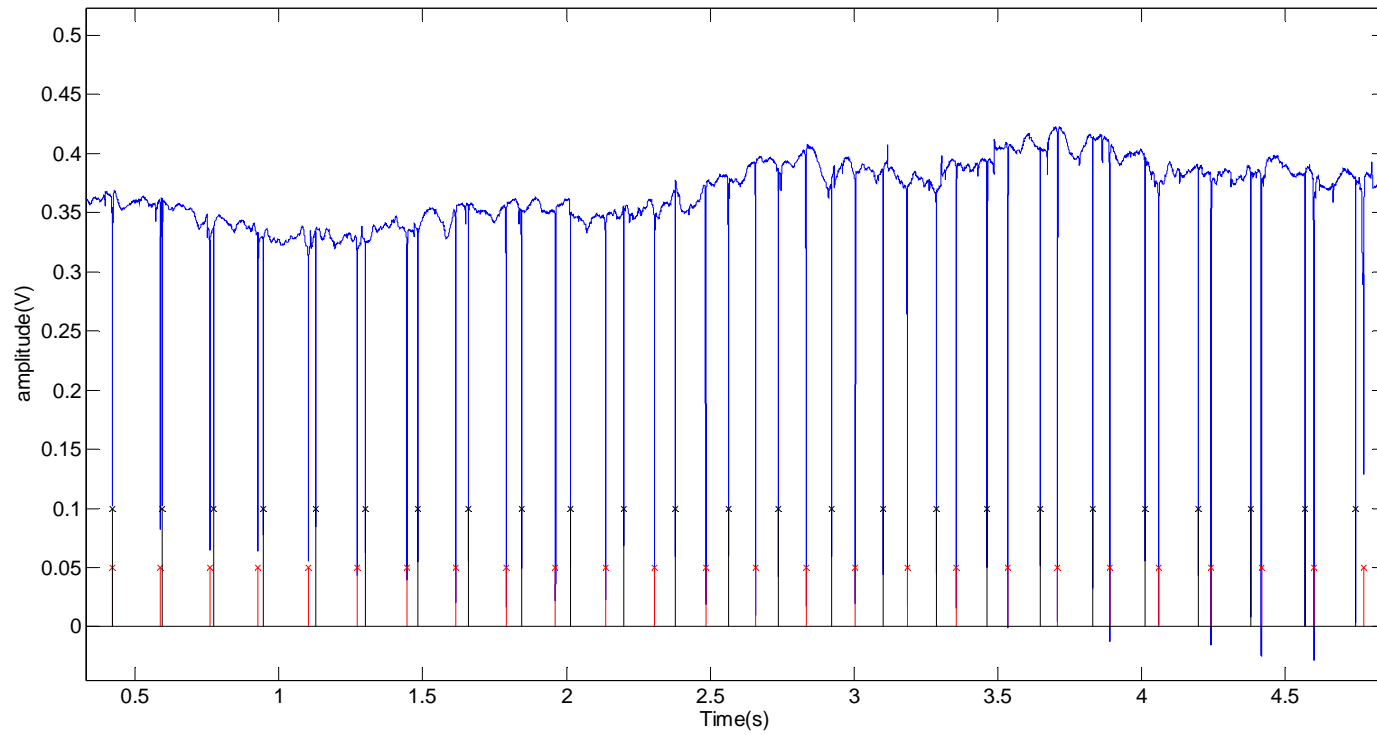
Figure 3.4 Transmission data captured by the oscilloscope. We have filtered the noise and the background by the digital filters. The two mode families are assigned separately as shown in the figure. One mode is assigned to red "x", while the other mode is assigned to black "x".

The mode family is assigned manually when the 2 modes cross each other. For this device, we observed that the Q factors of the two modes are different; thus, it is easy for us to organize the resonances to different mode families. We didn't observe any double peak in this transmission spectrum; however, we found that there is significant change in FSR evolution which is caused by the mode interaction phenomena. When the two resonances are close, it is observed that different mode families would interact with each other and change the local dispersion [3] [21] . Referring to figure 3.5(a) and (b), the last data of the FSR corresponds to the first 2 resonances in transmission spectrum in figure 3.4 since the tunable laser is sweeping from low to high wavelength. We observe a common FSR change in both mode 1 and 2. In order to obtain a better fit to the FSR evolution, we would not take those FSR data into account for the curve fitting. In addition, it is also observed that there is a significant FSR change at the first FSR data of mode 1. To understand why there is a significant FSR jump, we again check the resonance from transmission spectrum. The spectrum is shown in figure 3.6, and the zoom-in picture of the resonance corresponds to the first FSR data of mode 1 is shown in figure 3.6(b). It is found that there is a small extinction ratio resonance which is belonged to TM polarization. Therefore, we conclude that the significant FSR jump is result from the mode interaction between TE and TM polarization mode.
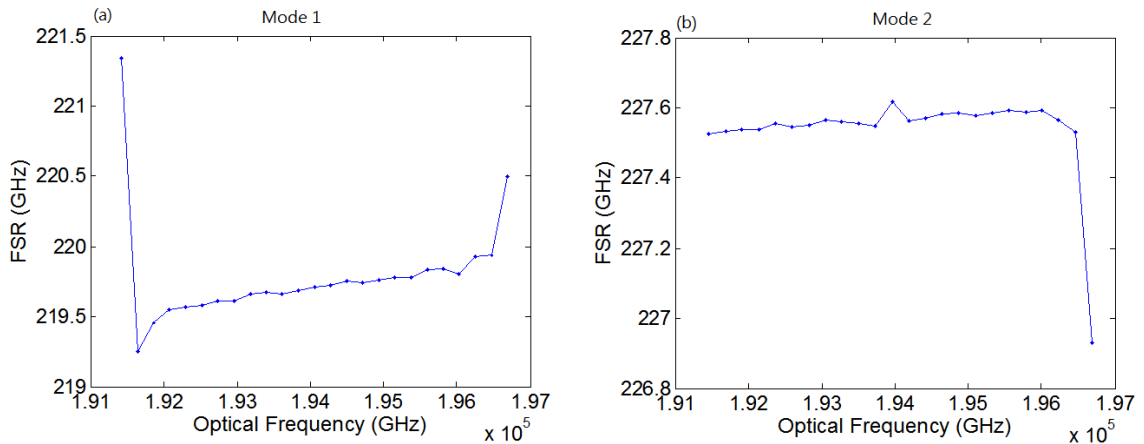
Figure 3.5 FSR evolution of the two modes from TE polarization. (a) FSR evolution of the mode family 1. We observe mode interaction in the first and last data. (b) FSR evolution of the mode family 2.
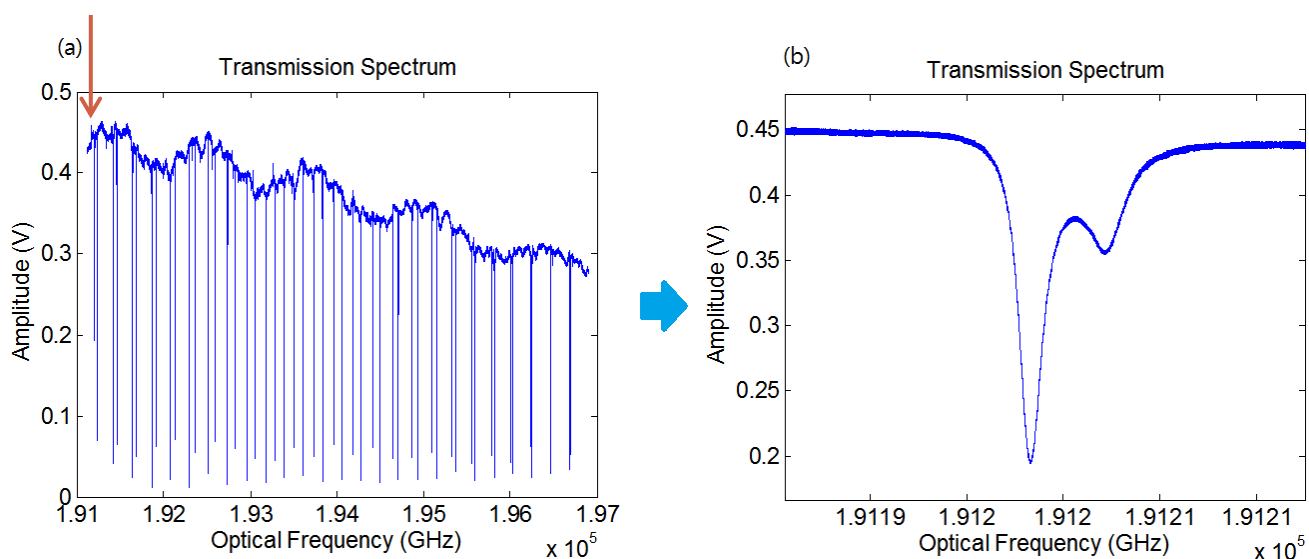
Figure 3.6 (a) Transmission spectrum of the micro-ring. The x-axis is the absolute frequency. (b) The first resonance of the transmission spectrum as indicated in (a). We found that there's a smaller extinction ratio resonance which corresponds to mode from TM polarization.
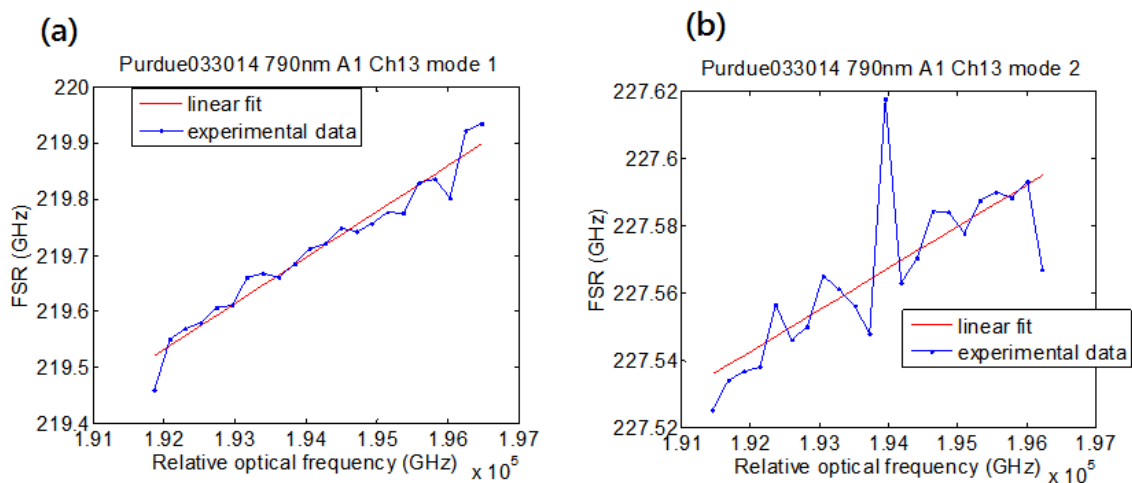
Figure 3.7 FSR evolution of the mode family 1 and 2 with mode interaction point excluded. Figure 3.5(a) is the FSR evolution of mode 1. (b) FSR evolution of mode 2

Finally, in figure 3.7, the FSR evolution and the curve fitted is shown. We found the dispersion of this micro-ring to be 337.55ps/km/nm for mode family 1 and 52.02ps/km/nm for mode 2.

Other measurement results are shown in table 3.1 and 3.2. We observe some agreement for the device with same dimension. However, we do have several measurements having different values for the same waveguide width and height. From table 3.1, we can see that the error tend to be higher if the waveguide width is wider. This is anticipated since with wider waveguide width, we would observe more modes in the transmission spectrum. This leads to more mode coupling and introduce more abrupt FSR change.

Table 3.1 Dispersion measurement of different devices. We see some agreement for the devices with same dimension. Some of the measurement has higher error since the FSR evolution is not well fitted.

|	Device	Waveguide Width (μm)	Waveguide Height (nm)	TE Mode 1 Dispersion(ps/ nm/km)	TE Mode 2 Dispersion(ps/n m/km)	TE Mode 3 Dispersion(p s/nm/km)
Purdue 033014 595nm	A1 Ch13	2	595	-61.99±15.77	16.68±24.31	
	A2 Ch5	2	595	-108.83±36.47	30.02±42.66	
	A2 Ch6	2	595	-79.68±44.02	-36.96±53.79	
	A2 Ch7	2	595	-90.86±17.35	-13.29±25.36	
	A2 Ch8	3	595	70.21±18.26	150.59±41.55	
	A2 Ch9	3	595	4.09±56.07	169.69±100.59	
Purdue 033014 790nm	A1 Ch12	2	790	39.27±7. 70	340.13±42.29	
	A1 Ch13	2	790	47.51±7. 74	336.18±14.04	
	A1 Ch19	3	790	4.85±41.27	144.42±37.22	452.28±107. 23
	A1 Ch19 drop port	3	790	-2.47±39.21	153.62±26.52	
	A2 Ch9	3	790		178.36±50.10	397.84±63.8 2
	A2 Ch10	3	790		161.62±38.19	411.8±79.81
	A2 Ch11	3	790		220.72±62.13	380.29±75.2

					2

Table 3.2 Dispersion measurement of different devices continued.

	Device	Waveguide Width (μm)	Waveguide Height (nm)	Mode 1 Dispersion(ps/nm/km)	Mode 2 Dispersion(ps/nm/km)
Purdue 072313 550nm	B4 Ch10	2	550		-789.26
	B4 Ch11	2	550	-538.13	-719.37
	B4 Ch11 drop port	2	550	-552.13	-729.36
	B4 Ch11 TM mode	2	550	-57.97	-204.65
Purdue 072313 800nm	B1 Ch4	2	800	100.31	
	B1 Ch4(2)	2	800	81.77±86.51	
	B4 Ch11	2	800	81.86±17.68	259.47±30.11
NIST	Gen5 Ch1	2	430	-1058.7±25.36	

In order to verify if our measurements are reasonable, we would like to compare the measured values to simulated ones. We ran the simulation with free software MIT Photonics Band (MPB). The total cavity dispersion includes the material dispersion and the geometry dispersion while the material dispersion is calculated based on Sellmeier's Equation. In addition, we assumed all waveguides has an etching angle of 5 degree. The comparison between simulation and measured dispersion is shown in table 3.3. From table 3.3, we do see some agreement between the measured and simulated dispersion. However, we found a great mismatch at waveguide height of 550nm and width of 2 μm. The possible reason for this mismatch is that the dispersion we measured might not be the fundamental mode.

Table 3.3Comparison between simulated dispersion and measured one

Waveguide Width (μm)	Waveguide Height (nm)	Simulated Dispersion(ps/nm/km)	Measured Dispersion(ps/nm/km)
2	550	-170	-538.13
2	600	-78	-108.83±36.47
2	800	59.9	47.51±7. 74
3	800	21.5	4.85±41.27

(a)
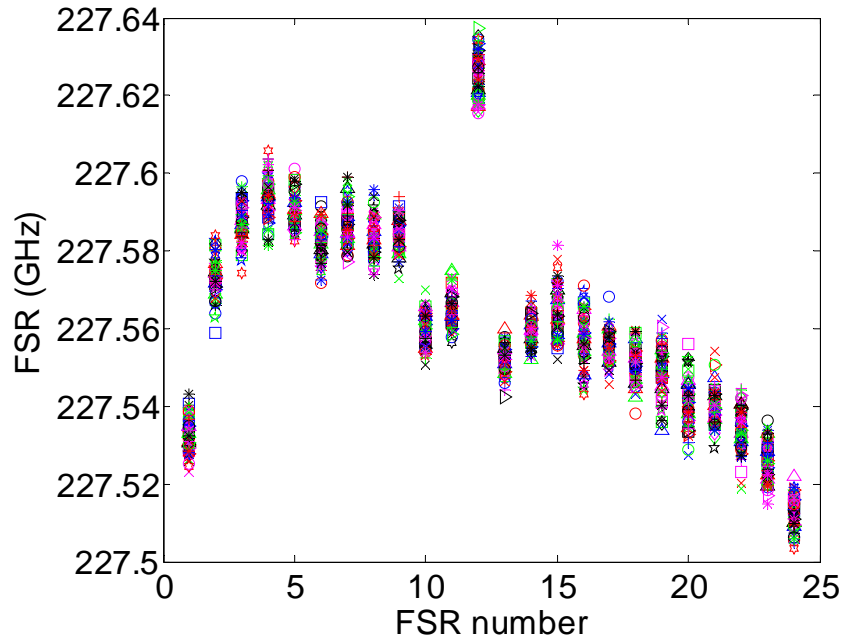
(b)

Figure 3.8 FSR error analysis for mode 1 (a)FSR deviations for the resonances from 1520nm to 1570nm from 70 measurements. The standard deviation of FSR is 4.7MHz. (b) Simulated dispersion by applying an error to each of the FSR. The error of the FSR is assumed to be the standard deviation.

(a)

(b)
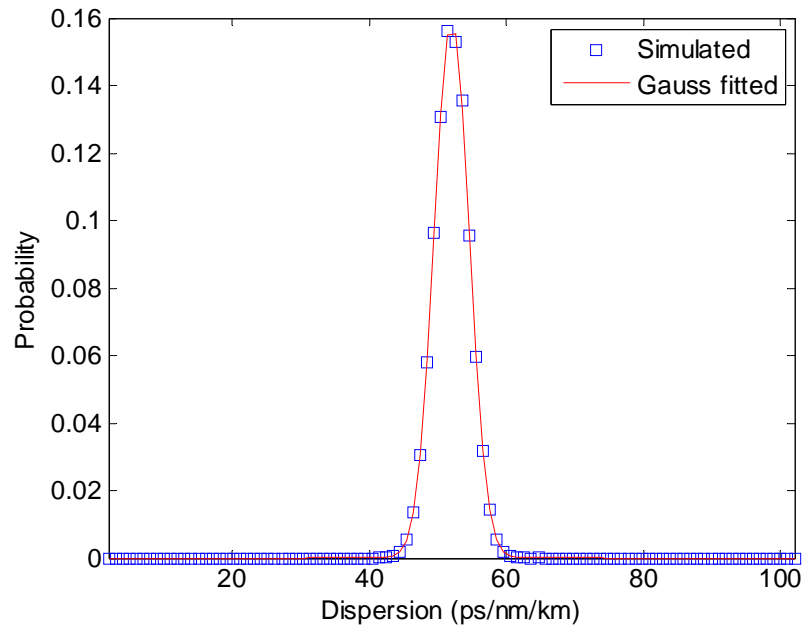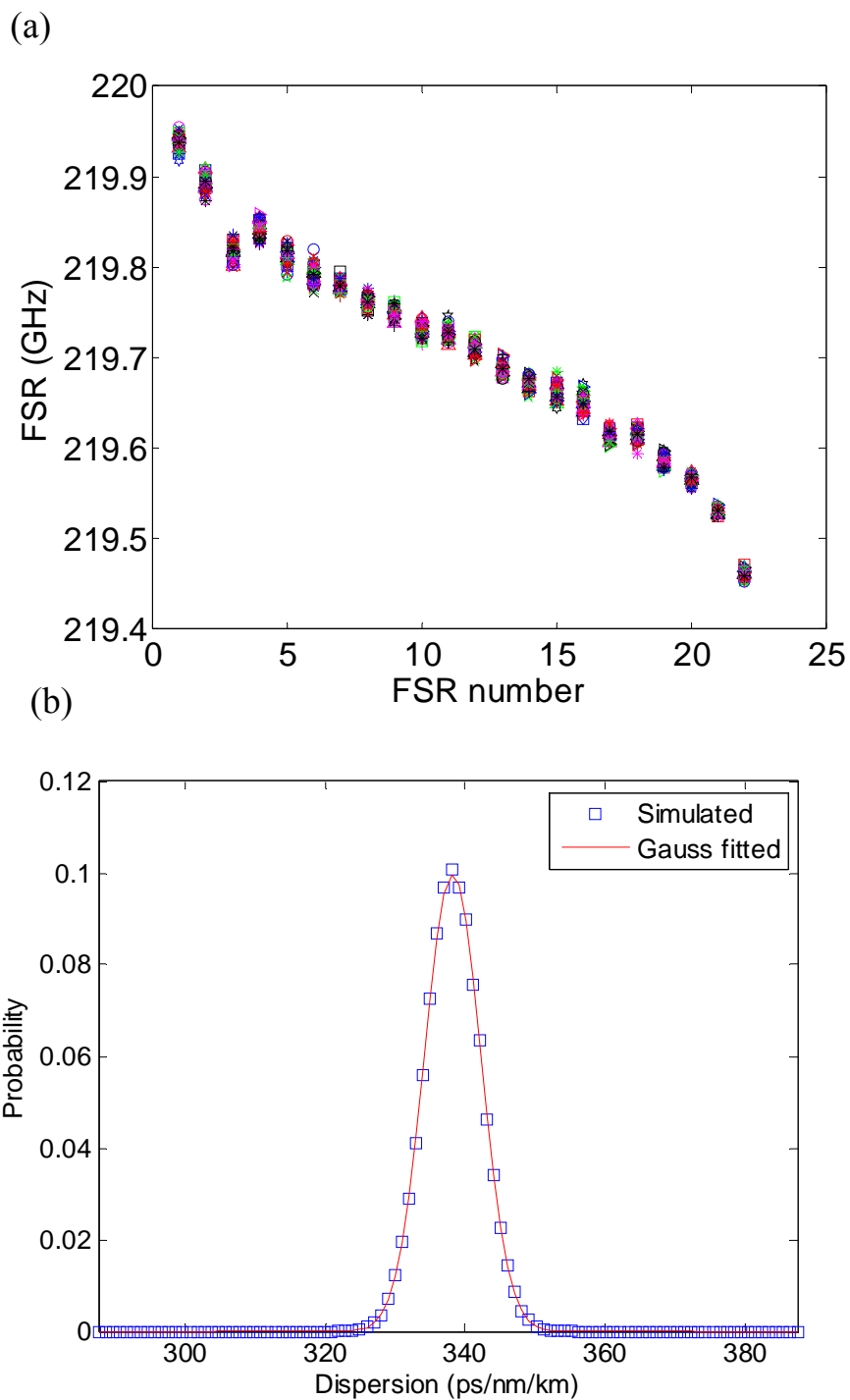

Figure 3.9 FSR error analysis for mode 1 (a)FSR deviations for the resonances from 70 measurements. The standard deviation of FSR is 6.24MHz. (b) Simulated dispersion by applying an error to each of the FSR. The error of the FSR is assumed to be the standard deviation.

3.2 Error Analysis of the Dispersion Measurement

In this section we would like to discuss the method we used to estimate the uncertainty of the dispersion measurement. In order to retrieve the uncertainty in our measurement, we performed measurement experiment on one micro-ring multiple times. The micro-ring we chose is channel 13 of Purdue 033014 790nm. The dimension of the chip is 790nm height, 2μm width, and the ring radius is 100μm. We maintained the same setup and performed the measurement 70 times. As discussed in section 3.1, we don't take the FSR that has mode interaction into account. The uncertainty of the FSRs for each mode family is shown in figure 38 and 3.9. In figure 3.8(a), the x-axis is the number of FSR we assigned to avoid ambiguity. We then found the standard deviation of FSRs σ_{FSR} to be 4.7MHz from the measurements. To estimate the uncertainty of dispersion, we assume each FSR has a normal distribution and simulate the curve fitting. We then simulate the FSR evolution and fit the curve for each of them and calculate the dispersion. The result is shown in figure 3.7(b). Finally, we choose the standard deviation of the dispersion value obtained previously as the uncertainty. For mode family 1 of this micro-ring, we find dispersion D = 52.02±2.52ps/nm/km. We perform similar process for mode family 2 and the result is shown in figure 3.8. The dispersion value and uncertainty is 337.55±4.11ps/nm/km.

Next we perform error analysis for Purdue B4 channel 11. The dimension of the chip is 800nm height, 2μm width, and the ring radius is 100μm. We did the measurement 30 times while setting the laser to sweep from 1540nm to 1560nm. The shorter sweeping range is chosen because the time it takes to save full range data is long. The deviation of each of the FSR is shown in figure 3.6. Again, we calculate the standard deviation of FSRs and simulate the FSR evolution. The error of the dispersion is determined by simulating the dispersion with the uncertainty of FSR we obtained. Figure 3.11 shows the simulation result with size of 50,000. Finally, we concluded the dispersion of this device is 81.82±17.68ps/nm/km.
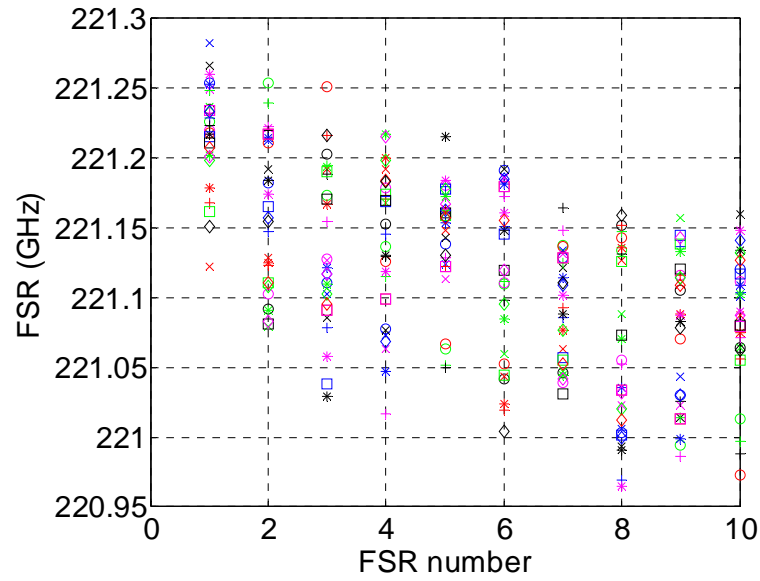
Figure 3.10 FSR deviations for the resonances from 1540nm to 1560nm. The maximum deviation of the FSR is around 200MHz.
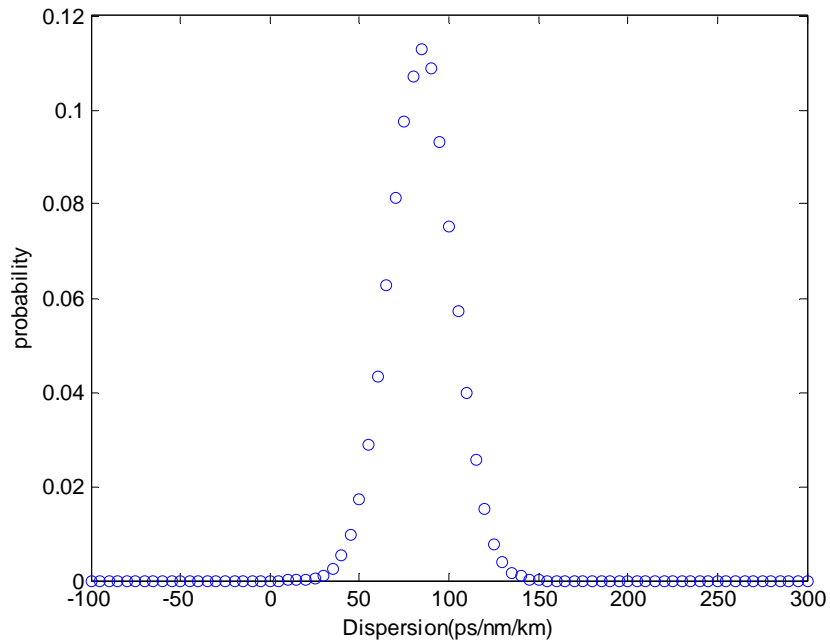

Figure 3.11 Dispersion simulations with size of 50,000. Again the error of FSR is assumed to be the standard deviation of FSR variation.

There are several factors that might contribute to the error. The first one is the nonlinearity of the laser sweep speed. Although we acquire the frequency markers and transmission spectrum synchronously, we still can't resolve the frequency between any 2 frequency markers. We used interpolation to find the relative frequency, but there is uncertainty if the laser sweep speed change abruptly. Another factor is the Q factor of the resonances. If the Q factor is higher, there is less error for the peak of the resonance, and we would expect a more accurate result. The noise in the transmission spectrum will introduce error to the dispersion as well, but it can usually be reduced with implementing digital low pass filter.

To verify how much error can be introduced by the laser sweep speed nonlinearity, we again measured another device – Purdue 072313 800nm B1 Ch4. Due to the fact that we choose arbitrary starting point of frequency marker and the data we obtained would shift a little bit in time scale in every measurement, there's an offset between different measurements. We chose a specific resonance as reference to align other resonances and find the offset. However, we found that the frequency variation of other resonances being around 400MHz to 500MHz. The variation is very large thus makes the measurement unreliable. Referring to table 2, the dispersion and error for this device is 81.77±86.51/nm/km. Although we can't find out why the error is large for this device, we do observe some devices would have greater uncertainty even they have same dimension.

For some of the device, we didn't perform multiple measurements. Therefore, we chose the difference between the fitted FSR and the experimental FSR data to be the variation of the FSR. Then we find the standard deviation of these variations and assumed it to be the error of FSRs. The error is usually found to be smaller. It is less reliable than the error we obtained from multiple measurements; however, we do see that when the FSR variation between fitted curve and actual data are larger, the errors we get from multiple measurements are larger as well. Therefore, it does provide an estimate of error we are going to expect.

3.3   Mode Interaction

If there is more than one mode family in the spectrum and they have different FSR, the modes would eventually cross in the transmission spectrum. From the experiment, we found that the FSR of the local resonances would be modified by the interaction between two modes. Figure 3.8 shows the result of mode interaction. We observe that the FSR of one mode suddenly increased while the FSR of the other mode decreased. The amount of FSR increased is similar to the amount decreased at the other mode. In addition, we observed that when two modes are close to each other, their Q factor will be modified as well. The mode with higher Q will have Q factor decreased while the mode with lower Q factor will exhibit higher Q factor. The mode interaction phenomenon is related to the initiation of micro-resonator frequency comb generation in normal group velocity dispersion [21].
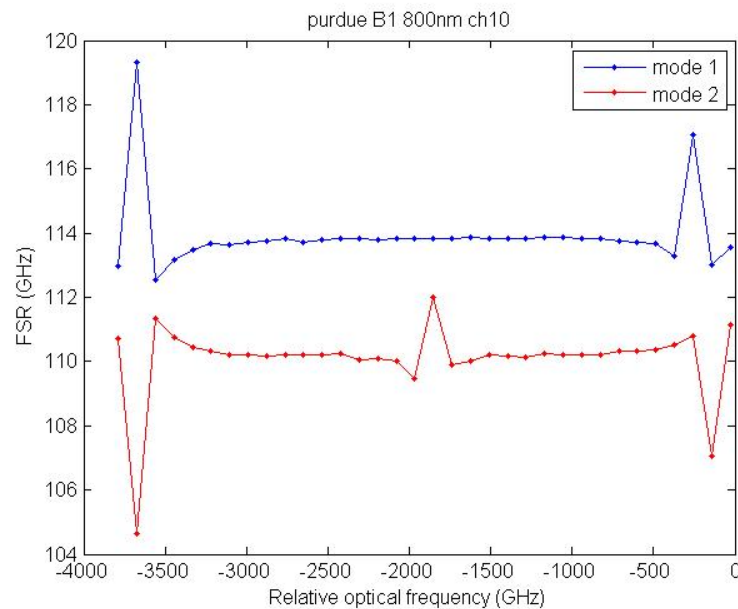
Figure 3.8 When there's mode interaction, a sudden FSR change is observed.

4. CONCLUSION AND FUTURE WORK

We have accomplished measuring the dispersion with the aid of frequency comb. We were able to implement signal processing algorithm to reduce the noise in the raw data and the dispersion of several different micro rings is measured. The accuracy of measurements is a very important factor and we are able to obtain an accurate measurement. Experimental result shows that we can measure the dispersion within 10% error for certain devices. In addition, we have found a good match between measured and simulated dispersion. However, there are several problems weren't solved.

First, we still observe large variation in FSR data for some of the devices. The large variation in FSR may result from the defect in micro rings. Secondly, we don't have a good match between simulation and experimental data for micro ring with 550nm waveguide height micro-ring. As mentioned above, the mismatch might come from that the simulated and measured dispersion was for different modes. Finally, although we can measure the dispersion with decent accuracy, it is possible to further increase the precision. Due to the fact that we only use 2 band-pass filters at 30MHz and 75MHz, we can't resolve the precision between any 2 markers. The interpolation method is used to increase accuracy but if laser sweep speed changes abruptly during 2 markers the accuracy is reduced. Therefore, it would be viable to add one more band-pass filter and reduce the frequency spacing between frequency markers. This will in turn increase the accuracy of the measurements.

LIST OF REFERENCES

LIST OF REFERENCES

[1]   T. Udem, R. Holzwarth, and T. W. Hansch, "Optical frequency metrology," *Nature,* vol. 416, pp. 233-237, 2002.

[2]   J. Reichert, M. Niering, R. Holzwarth, M. Weitz, T. Udem, and T. W. Hänsch,, "Phase Coherent Vacuum-Ultraviolet to Radio Frequency Comparison with a Mode-Locked Laser," *Physical Review Letters,* vol. 84, pp. 3232-3235, 2000.

[3]   Del'Haye, P. et al., "Frequency comb assisted diode laser spectroscopy for measurement of microcavity dispersion," *Nat Photon,* vol. 3, pp. 529-533, 2009.

[4]   J. A. Stone and P. Egan, "An Optical Frequency Comb Tied to GPS for Laser Frequency/Wavelength Calibration," *Journal of Research of the National Institute of Standards and Technology,* vol. 115, pp. 413-431, 2010.

[5]   C.-B. Huang, Z. Jiang, D. E. Leaird, and A. M. Weiner, " High-rate femtosecond pulse generation via line-by-line processing of phase-modulated CW laser frequency comb," *Electronics Letters,* vol. 42, pp. 1114-1115, 2006.

[6]   A. M. Weiner, Ultrafast Optics, John Wiley & Sons, Inc, 2008.

[7]   Del'Haye, P. et al., "Optical frequency comb generation from a monolithic microresonator," *Nature,* vol. 450, pp. 1214-1217, 2007.

[8]   T. J. Kippenberg, R. Holzwarth and S. A. Diddams, "Microresonator-based optical

frequency combs," *Science,* vol. 332, pp. 555-559, 2011.

[9] M. A. Foster, J. S. Levy, O. Kuzucu, K. Saha, M. Lipson, and A. L. Gaeta, "Silicon-based monolithic optical frequency comb source," *Optics Express,* vol. 19, pp. 14233-14239, 2011.

[10] T. Herr, K. Hartinger, J. Riemensberger, C. Y. Wang, E. Gavartin, R. Holzwarth, M. L. Gorodetsky & T. J. Kippenberg, "Universal formation dynamics and noise of Kerr-frequency combs in microresonators," *Nature Photonics,* vol. 6, no. 7, pp. 480-487, 2012.

[11] Ivan S. Grudinin et al., "Frequency comb from a microresonator with engineered spectrum," *Optics Express,* vol. 20, no. 6, pp. 6604-6609, 2012.

[12] P.-H. Wang, F. Ferdous, H. Miao, J. Wang, D. E. Leaird, K. Srinivasan, et al, "Observation of correlation between route to formation, coherence, noise, and communication performance of Kerr combs,," *Optics Express,* vol. 20, pp. 29284-29295, 2012.

[13] Victor Torres-Company et al., "Comparative analysis of spectral coherence in microresonator frequency comb," *Optics Express,* vol. 22, no. 4, pp. 4678-4691, 2014.

[14] P. Del'Haye, T. Herr, E. Gavartin, M. L. Gorodetsky, R. Holzwarth, and T. J. Kippenberg, "Octave Spanning Tunable Frequency Comb from a Microresonator," *Phys. Rev. Lett.,* vol. 107, no. 6, p. 063901, 2011.

[15] Yoshitomo Okawachi, Kasturi Saha, Jacob S. Levy et al., "Octave-spanning

frequency comb generation in a silicon nitride chip," *Optics Letters,* vol. 36, no. 17, pp. 3398-3400, 2011.

[16] T. Herr, V. Brasch, J. D. Jost et al., "Temporal solitons in optical microresonators," *Nature Photonics,* vol. 8, pp. 145-152, 2014.

[17] K. Saha, Y. Okawachi, B. Shim, J. Levy, R. Salem, A. Johnson, M. Foster, M. Lamont, M. Lipson, and A. Gaeta,, "Modelocking and femtosecond pulse generation in chip-based frequency combs," *Opt. Express,* vol. 21, no. 1, pp. 1335-1343, 2013.

[18] A. B. Matsko, A. A. Savchenkov, and L. Maleki, "Normal group-velocity dispersion Kerr frequency comb," *Optics Letters,* vol. 37, no. 1, pp. 43-45, 2012.

[19] L. Luo, G. Wiederhecker, K. Preston, and M. Lipson, "Power insensitive silicon microring resonators," *Opt. Lett.,* vol. 37, no. 4, pp. 590-592, 2012.

[20] Pei-Hsun Wang et al., "Drop-port study of microresonator frequency comb: power transfer, spectra and time-domain characterization," *Optics Express,* vol. 21, no. 19, pp. 22441-22452, 2013.

[21] Y. Liu, Y. Xuan, X. Xue, P. Wang, S. Chen, A. Metcalf, J. Wang, D. Leaird, M. Qi, and A. Weiner,, "Investigation of mode coupling in normal-dispersion silicon nitride microresonators for Kerr frequency comb generation," *Optica,* vol. 1, no. 3, pp. 137-144, 2014.

[22] Jiang Li et al., "Sideband spectroscopy and dispersion measurement in microcavities.," *Optics Express,* vol. 20, no. 24, pp. 26337-26344, 2012.

[23] Saha, Kasturi et al., "Modelocking and femtosecond pulse generation in chip-based

frequency comb," *Optics Express,* vol. 21, no. 1, pp. 1335-1343, 2013.

[24] Cyril Godey, Irina V. Balakireva, Aurélien Coillet, and Yanne K. Chembo, "Stability analysis of the spatiotemporal Lugiato-Lefever model for Kerr optical frequency combs in the anomalous and normal dispersion regimes," *Phys. Rev.,* vol. A 89, p. 063814, 2014.

[25] Lin Zhang et al., "Generation of two-cycle pulses and octave-spanning frequency combs in a dispersion-flattened micro-resonator," *Optics Letters,* vol. 38, no. 23, pp. 5122-5125, 2013.

APPENDIX

APPENDIX